

RESEARCH ARTICLE | JUNE 05 2012

Evidence for electric-field-driven migration and diffusion of oxygen vacancies in $\text{Pr}_{0.7}\text{Ca}_{0.3}\text{MnO}_3$

Zhaoliang Liao; Peng Gao; Xuedong Bai; Dongmin Chen; Jiandi Zhang

 Check for updates

Journal of Applied Physics 111, 114506 (2012)

<https://doi.org/10.1063/1.4724333>


View
Online


Export
Citation

CrossMark

Articles You May Be Interested In

Enhanced colossal electroresistance in $\text{Cu}/\text{Pr}_{0.7}\text{Ca}_{0.3}\text{MnO}_3/\text{Cu}$ structure

Journal of Applied Physics (November 2006)

Insulator–metal transitions in $\text{Pr}_{0.7}\text{Ca}_{0.3}\text{MnO}_3$ induced by a magnetic field

Appl. Phys. Lett. (January 1996)

Electroforming and endurance behavior of $\text{Al}/\text{Pr}_{0.7}\text{Ca}_{0.3}\text{MnO}_3/\text{Pt}$ devices

Appl. Phys. Lett. (September 2011)

Webinar

Boost Your Signal-to-Noise
Ratio with Lock-in Detection



Sep. 7th – Register now

 Zurich
Instruments

Evidence for electric-field-driven migration and diffusion of oxygen vacancies in $\text{Pr}_{0.7}\text{Ca}_{0.3}\text{MnO}_3$

Zhaoliang Liao,^{1,2} Peng Gao,² Xuedong Bai,² Dongmin Chen,^{2,a)} and Jiandi Zhang^{1,a)}

¹*Department of Physics and Astronomy, Louisiana State University, Baton Rouge, Louisiana 70810, USA*

²*Beijing National Laboratory for Condensed Matter Physics, Institute of Physics, Chinese Academy of Sciences, Beijing 100190, China*

(Received 16 February 2012; accepted 1 May 2012; published online 5 June 2012)

Combined *in situ* scanning probe microscopy with transmission electron microscope (TEM) has been used to study the field-induced migration of oxygen vacancies in the thin films of $\text{Pr}_{0.7}\text{Ca}_{0.3}\text{MnO}_3$. Local structural stripes which are associated with the existing oxygen vacancies in the material have been imaged *in situ* in real time with TEM and are found to migrate under external electric field. The stripes can also be induced by an electric field and relax as the field is dismissed. The characteristic decay time of field-induced stripes are found to be in the similar order of magnitude as the measured resistance relaxation time in the materials. These results confirm microscopically that oxygen migration plays a key role in the bipolar resistance switching behaviors in this class of oxide materials. © 2012 American Institute of Physics. [<http://dx.doi.org/10.1063/1.4724333>]

Electric field-induced resistance switching (RS) effect observed in sandwiched complex metal oxides has attracted prodigious interest due to its promising candidate for next generation non-volatile random access memory (NVRAM). Such an emergent resistance-based random access memory (ReRAM) cell is consisted of a capacitor-like structure in which an insulating/semiconducting oxide is sandwiched between two metal electrodes. Since 2000 when it was demonstrated that the narrow electric pulse can switch resistance of $\text{Pr}_{0.7}\text{Ca}_{0.3}\text{MnO}_3$ (PCMO) between high resistance and low resistance states,¹ a great effort has been paid to understand the underlying mechanism responsible for the observed functionality in this class of materials.^{2–6} In the case of unipolar RS in which the switching direction just depends on the amplitude of the applied voltage but not on the polarity, the formation/rupture of filamentary conducting path associated with the thermal redox and/or anodization near the interface between metal electrode and the oxide is considered to be the origin of RS.^{7–10} In bipolar-type RS where the switching direction depends on the polarity of the applied voltage, electrochemical migration of oxygen ions is regarded as the driving mechanism for bipolar RS.^{11–14} In many transition metal oxides, oxygen ion defects (typically oxygen vacancies) are present and much more mobile than cations. For either mechanism, it is extremely valuable to visualize the filament formation or anion (or vacancy) migration associated with the RS, thus driving many attempts to image directly or indirectly these processes microscopically.^{10,15–18} The observation of oxygen gas bubble formation at the anode suggests oxygen migration.¹¹ Both secondary-ion mass spectrometry (SIMS) analyses¹⁵ and TOF-SIMS secondary ion images¹⁶ indicate that the oxygen migration induces RS. The structure distortion along the conducting paths in TiO_2 and CeO_2 has been imaged by the transmission electron microscopy (TEM), which is assumed to be caused by the oxygen migration.^{10,17}

However, real-time imaging of oxygen motion or the related structural distortion driven by an external electric field is still absent.

Generally, it is hard to probe the active regions that respond for resistive switching, since they are normally in nanoscale size and buried between two metal electrodes due to special sandwiched metal/oxide/metal structure. The advanced TEM enables us to locally investigate the structure including chemical information, therefore, allows us to reveal the change of local structure related to RS. However, a special *in situ* setup with capability of nanoscale manipulation and applying local electric field simultaneously with structural imaging is needed. Along with this idea, we have developed an *in situ* TEM technique to fabricate RS devices inside TEM as schematically shown in Fig. 1(a). We used PCMO, one of the prototype RS materials, as a demonstration to illustrate possible microscopic pictures of electric-field-induced oxygen migration/diffusion. There are reports indicating that oxygen migration in PCMO plays the central role in RS.^{13,15,19,20} The resistance relaxation measurement also indicates that the oxygen diffuses in the RS process.¹³

Polycrystalline PCMO thin film was deposited on (111) orientated Pt/SiO₂/Si wafer with special back-biased face-target-sputtering technique at low temperature (<400 °C).¹⁹ The cross-section TEM specimen of PCMO thin film was first prepared by mechanical grinding and dimpling to ~1 μm thick at the center; then mounted to copper grid by using silver epoxy connecting the Pt to copper grid; and finally milled with 4–5 keV argon ion beam to be thin enough for TEM investigation. The thinnest area of the TEM specimen was ~30–100 nm thick.

An integrated *in situ* scanning probe microscopy (SPM) and TEM (SPM-TEM) system^{17,21} was used to perform the *in situ* measurements. A 3D piezomotor was integrated into TEM sample holder. A sharp tungsten-tip (W-tip) was used as SPM tip which can be finely approached to specific position of specimen with navigation of JOEL 2010 F operating at 200 kV. To enable the W-tip to contact the PCMO, we

^{a)}Authors to whom correspondence should be addressed. Electronic addresses: DongminChen@pku.edu.cn and jiandiz@lsu.edu.

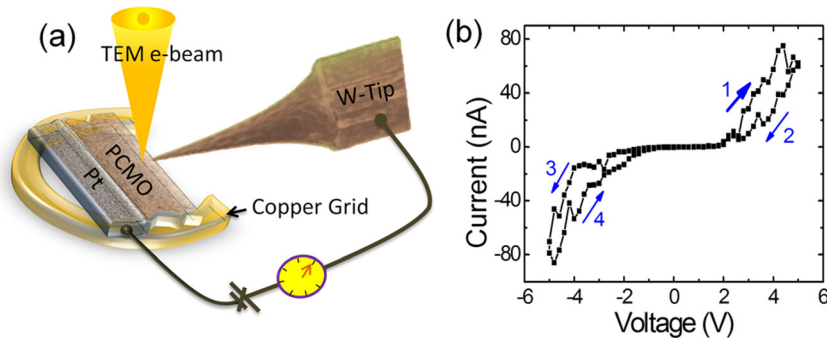


FIG. 1. (a) A schematic view of the *in situ* TEM characterization setup. The W-tip is controlled by a 3D piezomotor and Pt electrode is grounded. The SiO₂/Si substrate is not shown. (b) An *I-V* sweep loop (0 → 5 V → -5 V → 0) for W-tip/PCMO/Pt device measured inside TEM. The sweep sequence is 1 → 2 → 3 → 4.

chose the TEM specimen that has some parts of the PCMO without being covered with glue for tip contact. Furthermore, we cut off the copper grid in a way as shown in Fig. 1(a) schematically to allow the tip to approach the specimen. Then, the setup with the PCMO sample was mounted to the SPM-TEM sample holder and put into our TEM system. The bottom Pt layer was grounded through copper grid and the W-tip was used as the other electrode, so that the W-Tip/PCMO/Pt formed a two terminal device inside TEM. The *I-V* characteristics were measured with a Keithley 2400 sourcemeter. The constant voltage was also provided by Keithley 2400. The measurements with simultaneous TEM imaging were performed at room temperature.

With such a setup, we were able to perform simultaneously the TEM characterization to investigate the electric-field-driven structural evolution of devices. Fig. 1(b) shows the characteristic *I-V* sweep loop of W-tip/PCMO/Pt setup, evident for the bipolar RS character. Under positive bias, the system changes from low resistance to high resistance state. This is also confirmed by our independent conductive atomic force microscopy (AFM) measurement on similar implemented W-tip/PCMO/Pt setup.²⁰

The characteristic *I-V* hysteresis of W-tip/PCMO/Pt has been explained as the oxygen migration assisted interface oxidation/reduction of WO_x.²⁰ If the oxygen migration is the case to drive RS, it is expected to cause a local structural distortion along the migration path. To monitor the structure evolution in real time, we applied a constant bias to W-tip and then took a TEM image every ~ 1.0 s. The TEM image of W-tip/PCMO/Pt is shown in Fig. 2(a). The thickness of PCMO along the TEM electron beam direction is estimated to be less than 100 nm. The contact area between W-tip and PCMO is estimated about $100 \times 100 \text{ nm}^2$ and the distance from W-tip to the nearest part of the bottom Pt electrode is about 550 nm. Fig. 2(b) presents the zoom-in image of the region close to the W-tip before applying electric field. A stripe-ordered region with a spacing period of stripes of $\sim 3 d_{(001)_p}$ (P means primitive lattice in pseudo cubic phase so as to following text) is clearly revealed in the zoom-in image. We also observed similar stripe domains but with different stripe spacing. As we will discuss in the following, such a modulation stripe has been interpreted as an ordering of oxygen vacancies, where the stripe spacing depends on the local density of oxygen vacancies which exist in the film intrinsically.²²

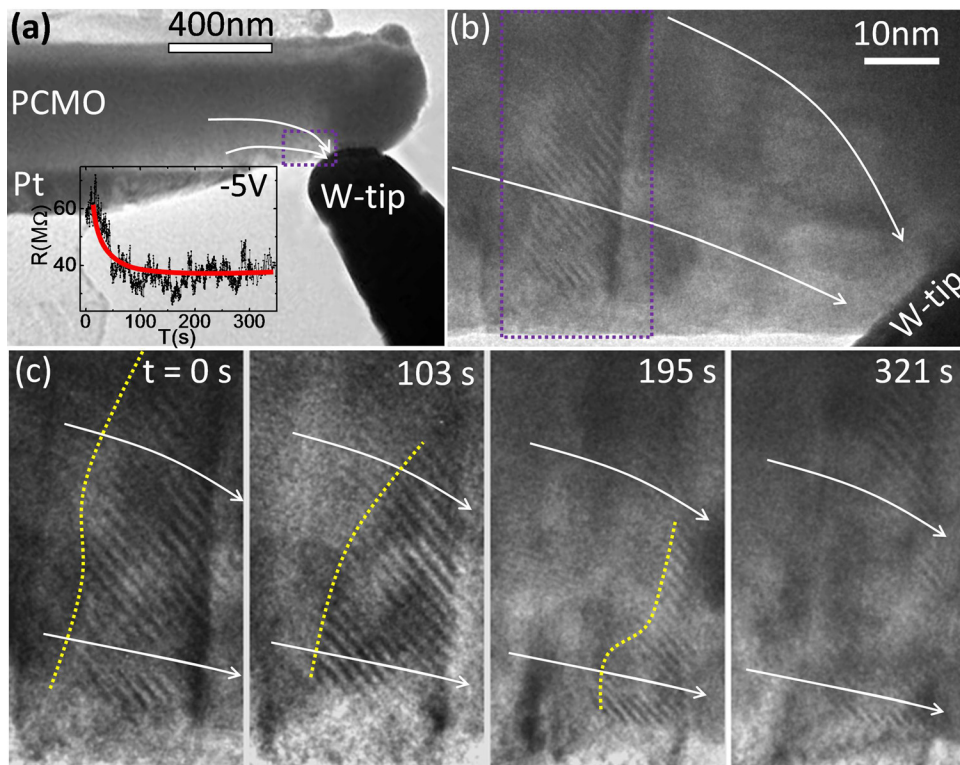


FIG. 2. (a) A TEM image of W-tip/PCMO/Pt devices. Inset is the resistance of the device versus time under -5 V bias and the thick solid line curve is used to show the trend. (b) A zoom-in image of the selected region of the PCMO film marked in (a). (c) A zoom-in and time-dependent image of selected region marked in (b) under the electric field applied through the W-tip. The field intensity is estimated $\sim 9 \times 10^6 \text{ V}\cdot\text{m}^{-1}$. The dot curves sketch the boundary of stripe domain. The white arrows indicate the electric field directions. An electron energy of 200 keV was used for TEM imaging.

Interestingly, both the structural modulation and consequently the electric transport can be tuned by applied external field. The resistance of the device versus time after applying a sample bias of -5 V is shown in the inset panel of Fig. 2(a). The large noise observed in R vs. T curve is due to instability at the *in situ* mechanical contact between W-tip and the film. The electric field can be roughly estimated as $E \sim 9 \times 10^6$ V·m $^{-1}$. The resistance decreased with time and started to saturate after ~ 50 s. A structure evolution near the tip was visualized simultaneously during applying the electric field. Fig. 2(c) displays a series of time-dependent images of structural modulation after applying the bias voltage. The boundary of the striped area indicated by a dashed yellow line gradually moved along the electric field direction. The stripes moved close to the tip and gradually faded away with time evolution. After about 321 s, the stripes were almost diminished. Therefore, we directly observed for the first time an electric-field-induced migration and evolution of stripes in PCMO film, which is correlated with the evolution of the device resistance.

In order to exclude the possible electron irradiation effect on the observed change of local structure, we monitored possible structure change of PCMO after half an hour of strong electron irradiation with a dose of $\sim 2 \times 10^6$ electrons·Å $^{-2}$ at a magnification of 500 k. We found no change of structure with such irradiation treatment. We also checked whether the structure change could be due to the stress from the W-tip contact. We found no change in structure in the TEM image with contacting W-tip but no applied bias. Thus, we conclude that the observed structure evolution in PCMO film (see Fig. 2) is solely due to the effect of the electric field.

To gain further insight into the local lattice dynamics associated with such an electric-field-induced oxygen vacancy migration, we have performed *in situ* measurements on the relaxation of electric-field-induced structural distortion/reconstruction. Figs. 3(a)–3(f) present a series of time-dependent

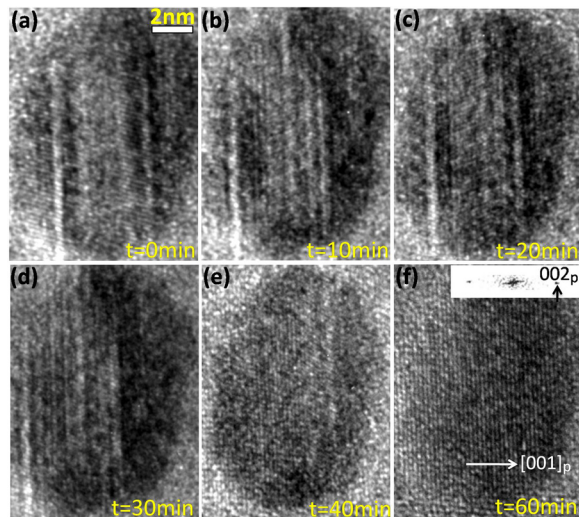


FIG. 3. A series of TEM images for the decaying electric-field-induced stripes in a crystalline grain of PCMO film. The evolution started right after the applied electric field ($\sim 9 \times 10^6$ V·m $^{-1}$) was removed. The crystalline orientation of the imaged grain is marked in panel (f). The inset is the corresponding FFT pattern.

images on the relaxation of the electric-field-induced stripe structure in a single crystalline grain of PCMO film after removing the external electric field through W-tip bias. The electric-field-induced vertical stripes in the grain gradually fade away with time and finally the crystalline grain restores its primary structure with no observable superstructure.

The relaxation time scale (referred as τ_s here after) for the observed stripes is estimated on the order of 1 h, profoundly longer than any simple electronic or structural relaxation, such as the melting of charge²³ or polaron ordering.²⁴ Such a slow relaxation should be related directly to the ion motion, i.e., oxygen vacancy diffusion. Based on the fact that when PCMO relaxes back to the thermal equilibrium state, the resistance should simultaneously become stable. The structure relaxation then should be responsible for the relaxation of the switched resistance. As shown in Fig. 4(a), an Ag-Paint/PCMO/Pt device with point contact between Ag nanoparticle and PCMO (Ref. 25) exhibits the same characteristic resistance switching behavior as Ag-tip/PCMO/Pt.²⁰ If only applying positive sweep loop, the resulted LRS then will slowly decay with relaxation time of 50 min [see Fig. 4(b)], which is indeed very close to τ_s . Nian *et al.* have also reported the same order of resistance relaxation time (~ 10 min) in this material and the resistance relaxation is thought to result from oxygen diffusion.¹³ The temperature-dependent resistance switching characteristics displayed in Figs. 4(c) and 4(d) also imply that the field induced switching is related to ion migration. The I - V hysteresis became smaller with decreasing temperature and completely disappeared below 140 K, even though a voltage sweep-loop with the maximum voltage of 10 V was applied (data not shown). Since the mobility of the oxygen ($\mu = \mu_0 e^{-E/(kT)}$) exponentially decays with increasing $1/T$, the oxygen will be frozen at low temperature. For example, $\mu(140$ K)/ $\mu(300$ K) is equal to $\sim 10^{-8}$ (here the activation energy (E) of 0.4 eV is used according to the result from Ref. 13). It can be interpreted that the freeze of oxygen causes the disappearance of RS. These results strongly suggest that both the observed electric field induced evolution of superstructure (Fig. 2) and the relaxation of the stripes (Fig. 3) are related to motion of oxygen vacancy in the system.

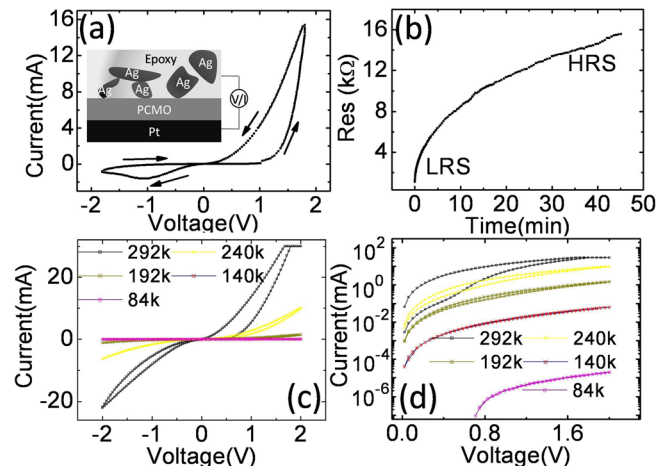


FIG. 4. (a) I - V hysteresis of Ag-Paint/PCMO/Pt; (b) Resistance relaxation after applying only positive sweep loop; Temperature-dependent I - V hysteresis in (c) linear and (d) logarithmic scale.

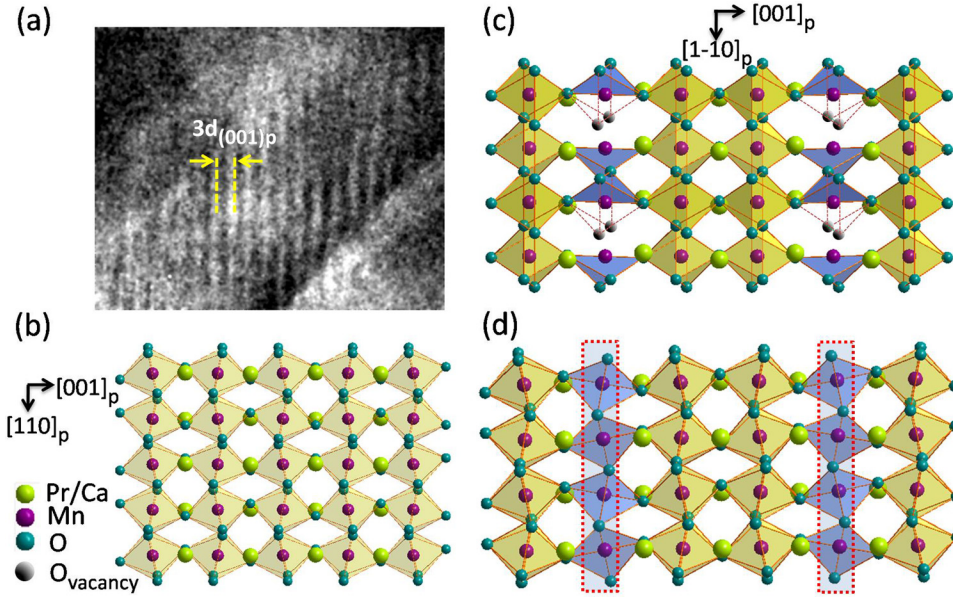


FIG. 5. (a) Zoom-in image of stripes in Fig. 2(c), showing a $p(3 \times 1)$ stripe superstructure along $[001]$ direction; (b) The structural model in $(1-10)_p$ -plane view of primitive lattice in pseudo cubic perovskite (ABO_3) structure; A possible $A_3B_3O_8$ oxygen vacancy model in (c) $(110)_p$ - and (d) $(1-10)_p$ -plane view.

We now interpret the *in situ* observed stripes as the superstructure associated with the local oxygen vacancy order and the formation and evolution of the stripes induced by an applied electric field result in the change of transport properties, including RS. With sufficient density, oxygen vacancies can self-assemble into certain orders and result in lattice reconstructions in this class of perovskite materials,^{22,26–29} such as the observed stripe modulation. An external electric field induced oxygen vacancy migration can change the local vacancy density and affect their self-assembling, resulting in the electric-field-induced superstructure evolution. Back in 1976, Grenier *et al.* proposed that oxygen vacancies in 3D cubic TMO perovskites [ABO_3 , as shown in Fig. 5(b)] could form $A_nB_nO_{3n-1}$ -type structure where $(n-1)$ octahedral planes alternate with one tetrahedral structure.²² According to the $A_nB_nO_{3n-1}$ model, oxygen vacancies prefer to locate on $\{001\}_P$ plane, and form strings along $\langle 110 \rangle_P$ direction, forming a modulated stripes with period of $nd_{(001)p}$. The $n=3$ and $n=4$ type reconstructions have been reported before.^{22,27–29} The high resolution image of the stripe in Fig. 3 shows that the field induced stripes locate in the (001) plane, consistent with the characteristic of oxygen vacancy order in perovskite materials. Although we do not have atomic-resolved images of stripes in Fig. 2, the measured distance of $\sim 3d_{(001)p}$ between stripes in PCMO (see Figs. 2 and 5(a)) implies that stripes have a modulation as $n=3$ case in the $A_nB_nO_{3n-1}$ model. A schematic model for these observed stripes is shown in Figs. 5(c) and 5(d). The oxygen vacancies in the $(001)_P$ plane form strings along $[110]_P$ direction. The planar view of reconstructed structure in the $(1-10)_P$ plane then gives rise to stripes with a period of $3d_{(001)p}$. The local oxygen vacancy density should manipulate the evolution of stripes, including possible change of periodicity and even orientation. Under an external electric field which influences the local oxygen vacancy density, the stripes will migrate, change their shape and orientation, depending on the strength and direction of local electric field (see Fig. 2).

Without the external field, the field induced a gradient of the concentration of oxygen vacancies will cause the field induced stripes relax as shown in Fig. 3. Yang *et al.* also reported similar phenomena in $SrTi_{0.2}Fe_{0.8}O_3$.²⁷

The structure evolution under electric field allows estimating the oxygen vacancy mobility. The drift velocity of oxygen vacancies should approximately equal that of stripes. The stripe boundary marked by a dashed yellow line in Fig. 2(c) moved ~ 14 nm in 321 s at an electric-field of $\sim 9 \times 10^6$ $V \cdot m^{-1}$, so the oxygen vacancy mobility is estimated to be $\mu = 4.8 \times 10^{-14}$ $cm^2 \cdot V^{-1} \cdot s^{-1}$. It is smaller than the reported value of 3.9×10^{-12} $cm^2 \cdot V^{-1} \cdot s^{-1}$ in Ref. 13. The smaller mobility probably resulted from different oxygen vacancy concentrations.¹³ The sample in Ref. 13 was grown to be oxygen deficient in oxygen free atmosphere and the resistivity of the low resistance state was reported to be $\sim 1.2 \times 10^5$ $\Omega \cdot cm$, three orders higher than that of our sample ($\sim 3.4 \times 10^2$ $\Omega \cdot cm$).¹⁹ The sample we have should have lower oxygen vacancy concentration, thus causing lower mobility as discussed in Ref. 13.

In summary, we present direct evidence for the dynamic migration and diffusion of oxygen vacancies in PCMO through *in situ* structural imaging, thus provide a microscopic view for the nature of RS functionality in this class of oxide materials. The manipulation of oxygen vacancy with external electric field not only controls the local chemical stoichiometry but also the structure, resulting in the change of the physical properties of TMOs, typically resistivity, for example. Although we use PCMO as a demonstration, the results should be general for other metal oxides and give insight into the development of oxide-based resistance random access memory.

This work was supported by a grant from the Chinese Academy of Sciences (No. KJCX2-SW-W26) and also by the National Natural Science Foundation of China under Grant No. 90406017. Z.L. and J.Z. were partially supported by U.S. DOE under Grant No. DOE DE-SC0002136.

- ¹S. Q. Liu, N. J. Wu, and A. Ignatiev, *Appl. Phys. Lett.* **76**, 2749 (2000).
- ²R. Waser and M. Aono, *Nature Mater.* **6**, 833 (2007).
- ³A. Sawa, *Mater. Today*, **11**, 28 (2008); references therein.
- ⁴R. Waser, *Microelectron. Eng.* **86**, 1925 (2009).
- ⁵R. Waser, R. Dittmann, G. Staikov, and K. Szot, *Adv. Mater.* **21**, 2632 (2009).
- ⁶H. Akinaga and H. Shima, *Proc. IEEE* **98**, 2237 (2010); references therein.
- ⁷J. F. Gibbons and W. E. Beadle, *Solid-State Electron.* **7**, 785 (1964).
- ⁸K. Kinoshita, T. Tamura, M. Aoki, Y. Sigiya, and H. Tanaka, *Appl. Phys. Lett.* **89**, 103509 (2006).
- ⁹H. D. Lee, B. Magyari-Köpe, and Y. Nishi, *Phys. Rev. B* **81**, 193202 (2010).
- ¹⁰D.-H. Kwon, K. M. Kim, J. H. Jang, J. M. Jeon, M. H. Lee, G. H. Kim, X.-S. Li, G.-S. Park, B. Lee, S. Han, M. Kim, and C. S. Hwang, *Nat. Nanotechnol.* **5**, 148 (2010).
- ¹¹K. Szot, W. Speier, G. Bihlmayer, and R. Waser, *Nature Mater.* **5**, 312 (2006).
- ¹²M. Janousch, G. I. Meijer, U. Staub, B. Delley, S. F. Karg, and B. P. Andreasson, *Adv. Mater.* **19**, 2232 (2007).
- ¹³Y. B. Nian, J. Strozier, N. J. Wu, X. Chen, and A. Ignatiev, *Phys. Rev. Lett.* **98**, 146403 (2007).
- ¹⁴J. J. Yang, F. Miao, M. D. Pickett, D. A. A. Ohlberg, D. R. Stewart, C. N. Lau, and R. S. Williams, *Nanotechnology* **20**, 215201 (2009).
- ¹⁵D. J. Seong, M. Hassan, H. J. Choi, J. Y. Lee, J. S. Yoon, J. B. Park, W. T. Lee, M. S. Oh, and H. S. Hwang, *IEEE Electron Device Lett.* **30**, 919 (2009).
- ¹⁶C. Yoshida, K. Kinoshita, T. Yamasaki, and Y. Sugiyama, *Appl. Phys. Lett.* **93**, 042106 (2008).
- ¹⁷P. Gao, Z. Z. Wang, W. Y. Fu, Z. L. Liao, K. H. Liu, W. L. Wang, X. D. Bai, and E. G. Wang, *J. Micron* **41**, 301 (2009).
- ¹⁸B. Bryant, Ch. Renner, Y. Tokunaga, Y. Tokura, and G. Aepli, *Nat. Commun.* **2**, 212 (2011).
- ¹⁹Z. L. Liao, Z. Z. Wang, Y. Meng, Z. Y. Liu, P. Gao, J. L. Gang, H. W. Zhao, X. J. Liang, X. D. Bai, and D. M. Chen, *Appl. Phys. Lett.* **94**, 253503 (2009).
- ²⁰J. L. Gang, S. L. Li, Y. Meng, Z. L. Liao, X. J. Liang, and D. M. Chen, *Chin. Phys. Lett.* **27**, 027301 (2009).
- ²¹P. Gao, Z. Z. Wang, K. H. Liu, Z. Xu, W. L. Wang, X. D. Bai, and E. G. Wang, *J. Mater. Chem.* **19**, 1002 (2009).
- ²²J. C. Grenier, J. Darriet, M. Pouchard, and P. Hagenmuller, *Mater. Res. Bull.* **11**, 1219 (1976).
- ²³K. Miyano, T. Tanaka, Y. Tomioka, and Y. Tokura, *Phys. Rev. Lett.* **78**, 4257 (1997).
- ²⁴C. Jooss, L. Wu, T. Beetz, R. F. Klie, M. Beleggia, M. A. Schofield, S. Schramm, J. Hoffmann, and Y. Zhu, *Proc. Natl. Acad. Sci. U. S. A.* **104**, 13597 (2007).
- ²⁵M. Fujimoto, H. Koyama, Y. Nishi, and T. Suzuki, *Appl. Phys. Lett.* **91**, 223504 (2007).
- ²⁶A. G. Khachaturyan, *Theory of Structural Transformations in Solids* (Wiley, New York, 1983), pp. 511–523.
- ²⁷Y. G. Wang, S. Steinsvik, R. Høier, and T. Norby, *J. Mater. Sci. Lett.* **14**, 1027 (1995).
- ²⁸J. M. González-callbet and M. Vallet-Regí, *J. Solid State Chem.* **68**, 266 (1987).
- ²⁹J.-C. Grenier, G. Schiffmacher, P. Caro, M. Pouchard, and P. Hagenmuller, *J. Solid State Chem.* **20**, 365 (1977).